Frontiers in Bioscience Landmark

Front. Biosci. (Landmark Ed) **2025**; 30(12): 46692
https://doi.org/10.31083/FBL46692

Original Research

Hypoxia-Activated PERK Promotes Epithelial-Mesenchymal Transition in Gliomas: A Single-Cell and Spatial Transcriptomic Study With Therapeutic Implications

Jingyan Gu[1,2,†], Yue Kong[3,†], Yaohua Liu[1,2], Xu Wang[2], Hongyu Tang[1,2], Tingting Zang[2], Jian Yin[2,*], Lianping Gu[2,4,*]

[1]Department of Neurosurgery, Shanghai General Hospital Affiliated to Shanghai Jiao Tong University School of Medicine, Shanghai Jiao Tong University, 200080 Shanghai, China
[2]Department of Neurosurgery, Shanghai General Hospital, 200080 Shanghai, China
[3]Department of Oral Basic Medicine, Hospital of Stomatology, Sun Yat-sen University, 510062 Guangzhou, Guangdong, China
[4]Department of Neurosurgery, Shanghai General Hospital Affiliated to Nanjing Medical University, Nanjing Medical University, 210029 Nanjing, Jiangsu, China
*Correspondence: dr_yin@163.com (Jian Yin); gulianping2025@163.com (Lianping Gu)
[†]These authors contributed equally.
Academic Editors: Erika Di Zazzo and Seok-Geun Lee
Submitted: 17 September 2025 Revised: 6 November 2025 Accepted: 21 November 2025 Published: 17 December 2025

Abstract

Background: Glioma, the most common brain tumor in adults, exhibits marked hypoxia and invasiveness. Endoplasmic reticulum stress (ERS) and the unfolded protein response (UPR) have been implicated in tumor progression, while epithelial mesenchymal transition (EMT) drives invasion and metastasis. **Methods**: This study explored the role of ERS, particularly the PKR-like endoplasmic reticulum kinase (PERK) pathway, in promoting EMT and malignancy in glioma. Based on publicly available bulk transcriptomic data, we analyzed PERK activity in high-grade and hypoxic gliomas. PERK activation across glioma subtypes was compared using publicly available single-cell sequencing, and its correlation with EMT upregulation was evaluated using pseudotime analysis. The effects of PERK on glioma migration and invasion in a hypoxic environment were investigated using PERK-silenced glioma cell lines. *In vivo* tumorigenicity was assessed in nude mice by measuring tumor size and EMT marker expression. Intercellular communication was examined using CellChat analysis. Hypoxic niche regions were identified using publicly available spatial transcriptomics with PERK-EMT co-localization. **Results**: Hypoxia-induced PERK activation promoted EMT, enhancing glioma cell migration and tumor growth. High PERK signatures correlated with EMT activation in aggressive gliomas. Genetic silencing of PERK reduced the expression of EMT-related proteins, an effect partially reversed by hypoxia. Inhibition of PERK signaling decreased tumor size in mice. PERK-activated glioma subpopulations exhibited stronger cell–cell communication through secreted phosphoprotein 1 (SPP1)-CD44 interactions. Spatial transcriptomic analysis confirmed enrichment of the PERK/EMT pathway in hypoxic niches alongside SPP1-CD44 co-localization. **Conclusion**: These findings reveal PERK-driven EMT as a key mechanism linking ER stress to glioma progression, with hypoxia reinforcing this axis. Targeting the PERK signaling axis or SPP1-CD44 interactions may offer novel therapeutic strategies against aggressive gliomas.

Keywords: glioma; epithelial-mesenchymal transition; hypoxia; endoplasmic reticulum stress; PERK kinase

1. Introduction

Glioma, the most prevalent and aggressive brain tumor in adults, is defined by cellular heterogeneity with diverse subtypes and gene expression patterns [1,2]. It also possesses the capacity for rapid growth and extensive angiogenesis under hypoxic conditions. The tumor microenvironment of glioma is complex, characterizing hypoxia, nutrient deprivation, and immune suppression, all of which collectively influence tumor growth and treatment responses [3]. The processes of epithelial-to-mesenchymal transition (EMT) and endoplasmic reticulum stress (ERS) are crucial processes closely associated with the hypoxic microenvironment in glioma progression [4,5]. Although these signaling pathways highlight invasive, migratory, and malignant gliomas, the regulatory mechanisms associated with these proteins remain unclear. EMT is a fundamental biological process where cells undergo extensive biochemical changes, acquiring a mesenchymal phenotype with reduced cell adhesion and increased migratory capability [6] through the modulation of various epithelial markers such as E-cadherin, cytokeratin, laminin-1, and desmoplakin, as well as mesenchymal markers including vimentin, fibronectin, N-cadherin, Twist, Snail, and Slug [7]. In glioblastoma, multiple signaling pathways tightly regulate EMT, and hypoxia exacerbates migration and invasion by promoting this mesenchymal transition [8]. The mesenchymal subtype of glioma is closely associated with poor prognosis [9]. Targeting the hypoxic microenvironment may

attenuate EMT in gliomas, thereby holding promise for glioma treatment [10].

In recent years, evidence suggests that the ERS response and its associated unfolded protein response (UPR) signals govern tumor cell migration, invasion, angiogenesis, and inflammation [11]. As a key branch of the UPR, PKR-like endoplasmic reticulum kinase (PERK) signaling is activated by phosphorylating eukaryotic initiation factor 2α (eIF2α), which globally attenuates protein synthesis to alleviate proteotoxic burden. Additionally, this pathway selectively promotes the translation of transcription factors such as ATF4, thereby driving the expression of genes involved in antioxidant responses, amino acid metabolism, and autophagy, enabling cellular adaptation under stress. In the context of cancer, PERK signaling plays a key role in progression, proliferation, and resistance to chemotherapy [5,12]. Hypoxia in tumors promotes PERK signaling, coordinating several downstream signaling factors, including glucose-regulated protein 78 (GRP78) [13]. In colorectal cancers, PERK inhibition is shown to suppress SLC7A11 expression, and sensitize cancer cells to lipid peroxidation, leading to ferroptosis [14]. Thus, targeting PERK represents a potential strategy for treating tumors. The PERK signaling pathway regulates the tumor microenvironment by promoting the production of pro-inflammatory and pro-angiogenic cytokines and chemokines [15,16], such as the stimulation of vascular endothelial growth factor A (VEGFA) secretion from tumor cells upon binding of VEGF to VEGFR1 [17].

CD44 is a widely recognized marker of glioma stem cells, extensively expressed in the mesenchymal subtype of gliomas, and is associated with poor prognosis [18]. Inhibiting CD44 can reduce hypoxia-induced stemness in gliomas, thereby exerting therapeutic effects [19]. Secreted phosphoprotein 1 (SPP1), as a chemokine, regulates cell adhesion, movement, and activation in cancers, including gastric, liver, and pancreatic cancers, causing tumor progression and metastasis [20–22]. SPP1+macrophages are now considered immune barriers in liver cancer immunotherapy and influence treatment outcomes [23]. The SPP1-CD44 signaling pathway is implicated in gliomas and closely associated with the PI3K/Akt and related pathways [24].

This study aimed to comprehensively investigate the mechanisms by which hypoxia-induced ERS promotes glioma progression, utilizing a multi-omics approach. Our objectives included analyzing multi-dimensional transcriptomic data from publicly available datasets, performing functional assays in cell lines and animal models, and evaluating spatial interactions within the tumor microenvironment to elucidate the underlying pathways. In summary, our studies revealed that PERK pathway activation in glioma cells under hypoxic conditions is accompanied by EMT, which promotes invasion, migration, and malignant transformation of gliomas. Using single-cell sequencing, we explored changes in the hypoxia-induced PERK activation and EMT pathways in glioma cells, and their interactions with non-tumor cells in the tumor microenvironment. Spatial transcriptomics confirmed that hypoxic regions enriched with PERK-activated tumor cells exhibit heightened EMT pathway activation, accompanied by co-localization of SPP1 and CD44. Silencing PERK decreased EMT pathway activity, and our established mouse model further demonstrated the therapeutic potential of targeting the PERK pathway for glioma. Overall, our research uncovers novel mechanisms underlying glioma invasion, migration, and progression, offering new insights and potentially effective treatment strategies.

2. Materials and Methods

2.1 Data and Gene Set Acquisition

Bulk RNA-seq data were obtained from the Chinese Glioma Genome Atlas (CGGA, http://www.cgga.org.cn/), specifically dataset mRNAseq_325, which includes transcriptomic and clinical data from 325 glioma samples. For specific analyses, subsets of samples were used according to World Health Organization (WHO) grades: 103 Grade II, 79 Grade III, and 139 Grade IV cases [25]. Single-cell RNA-seq data were sourced from the Gene Expression Omnibus (GEO, https://www.ncbi.nlm.nih.gov/geo/) dataset GSE182109, from this cohort, we selected newly diagnosed glioblastoma (ndGBM) and low-grade glioma (LGG) samples for downstream analysis. It is noteworthy that a key commonality between the CGGA bulk dataset and this single-cell dataset is the inclusion of glioma samples across different grades, enabling multimodal exploration of our research questions [25–27]. Spatial transcriptomics data from Datadryad (https://doi.org/10.5061/dryad.h70rxwdmj) were accessed. Gene sets related to EMT and hypoxia were retrieved from the HALLMARK database (https://www.gsea-msigdb.org/gsea/msigdb/index.jsp), while those associated with PERK signaling were obtained from the REACTOME database (https://curator.reactome.org/) [28–30].

2.2 Gene Set Variation Analysis (GSVA) Scoring and Visualization

PERK, EMT, and hypoxia Gene sets from the HALLMARK and REACTOME databases were employed to transform the expression matrix of glioma samples from the CGGA dataset into enrichment score (ES) matrices using the R package in RStudio R 4.1.2 (R Core Team, Vienna, Austria). This process generated GSVA enrichment scores for each gene set across all samples, which were visualized using the ComplexHeatmap 2.13.1 (Guangchuang Yu, Hong Kong, China).

2.3 Survival Analysis

Clinical data and PERK scores from the CGGA database were used to perform survival analysis. Statisti-

cal analyses and survival data visualization were conducted using the R package survival in RStudio.

2.4 Differential Gene Analysis and Protein-Protein Interaction (PPI) Network Analysis

Differential gene expression analysis on transcriptome count data was conducted between two groups, with the reference group designated as "Low". The DESeq2 1.43.0 (Michael Love, Berkeley, CA, USA) was used to identify differentially expressed genes on the raw count matrix, following standard procedures. Differential expression was visualized through volcano plots using ggplot2 3.4.2 (Hadley Wickham, New Zealand). Next, PPI network analysis was performed using the STRING database (https://string-db.org) on the top 100 upregulated genes identified in the high PERK score group from the CGGA database [31]. Finally, we utilized igraph for data processing, including data cleaning and organization, followed by visualization of the network graph by using ggraph.

2.5 Gene Set Enrichment Analysis (GSEA) and Deconvolution Analysis

We conducted GSEA on the differentially expressed genes, including Gene Ontology (GO), Kyoto Encyclopedia of Genes and Genomes (KEGG), and Hallmark pathways, using gene sets from the MSigDB Collections [29]. Initially, molecular identifiers in the input data were converted to ensure compatibility with gene set databases. Subsequently, we employed the clusterProfiler 4.2.2 (Guangchuang Yu, Hong Kong, China) in R to perform GSEA. GSEA results were visualized to identify enriched pathways. In addition, we computed immune infiltration levels in the CGGA dataset using the ssGSEA Algorithm from the GSVA 1.42.0 (Robert K. Gideons, Barcelona, Catalonia, Spain), based on markers for 24 immune cell types [32].

2.6 Dimensionality Reduction, Clustering, and Cell Annotation

We analyzed single-cell RNA sequencing data using the Seurat package in R 4.1.2 (R Core Team, Vienna, Austria) by RStudio 2021.09.1 Build 372 (Posit, Boston, MA, USA). Initially, genes expressed in fewer than three cells and cells expressing fewer than 100 genes were filtered out. Next, the RemoveDoublets function was applied to eliminate 4% of doublets, followed by exclusion of samples with mitochondrial gene expression exceeding 10%. Gene expression variability was determined using Seurat's FindVariableFeatures function. Dimensionality reduction was performed with Principal Component Analysis (PCA), and batch effects were corrected using the RunFastMNN algorithm. UMAP clustering identified 26 distinct clusters; cell types were annotated by integrating reported and highly variable marker genes. Tumor cell subclusters were then extracted for further dimensionality reduction and clustering using t-Distributed Stochastic Neighbor Embedding (tSNE). The annotation of glioma cell subtypes was based on gene sets and signature genes provided by previously published literature [33].

2.7 AddMoudleScore Analysis

We analyzed the single-cell transcriptome data by employing the AddMododuleScore method to assess the activity of specific gene expression modules at the cellular level. This method transforms gene expression data into numerical scores that reflect the involvement of each cell in the target biological processes. Results were visualized using ggplot2.

2.8 Pseudo-Temporal Analysis

We utilized the to conduct Pseudo-temporal analysis of tumor cell populations using machine learning methods were performed using the monocle2 2.22.0 (Cole Trapnell, Seattle, WA, USA) [34]. Changes in the expression of key marker genes associated with the EMT- and hypoxia-related marker genes were observed along their transitions in tumor cell subpopulations.

2.9 CellChat Analysis

Cell-cell interactions between PERK-activated glioma cells and their immune microenvironment were explored using the CellChat 1.6.1 (Suoqin Jin, Hong Kong, China) [35]. Intercellular communication was simulated interactions involving ligands, receptors, and their respective auxiliary factors were evaluated. Signaling pathways were visualized using the "netVisual_aggregate" function. Ligands and receptors were categorized as outgoing and incoming signals, respectively.

2.10 Spatial Transcriptomics Analysis

We utilized the Seurat package in RStudio (version 4.1.2), to read and assess spatial transcriptomics data. Data were normalized using SCTransform, ensuring robustness in downstream analyses. We assigned pathway scores to each spatial spot through AddMoudleScore, allowing the evaluation of pathway activities across spatial locations. Gene and pathway expression were visually represented using SpatialFeaturePlot in Seurat 4.3.0 (Satija Lab, NY, USA).

2.11 SPOTlight Deconvolution and Correlation Analysis

Single-cell RNA sequencing data were deconvoluted into spatial transcriptomics data using the SPOTlight method. Gene expression matrices for each cell were extracted from our single-cell RNA sequencing data. We integrated spatial information and gene expression patterns employing SPOTlight to map single-cell data onto a spatial grid and visualize it using spatial feature plots. Furthermore, the relationship between the proportion of glioma

cells with high activation of PERK and the EMT score in each SPOT was investigated through correlation analysis.

2.12 Cell-Line Acquisition and Culture

The glioma cell lines (LN229) obtained from Procell Life Science & Technology Co., Ltd. (Wuhan, China). These cell lines were cultured in a 5% O_2 normal oxygen cell incubator and a 1% O_2 hypoxia cell incubator according to the experimental protocol. Next, the shPERK lentivirus was transduced into glioma cells, which were expanded to the required number, and a stably transfected PERK-low-expression glioma cell line was selected. The cells were randomly categorized into the negative control and the experimental groups. All cell lines were validated by STR profiling and tested negative for mycoplasma.

2.13 Cell Infection and Construction of Lentiviral Vector

PERK and negative control (NC) shRNAs were first constructed according to the effective PERK shRNA (5′-GCAGGUCAUUAGUAAUUAU-3′) and NC sequences (5′-UUCUCCGAACGUGUCACGU-3′), which were validated in this study. For transient transfection experiments, PERK and negative control (NC) shRNAs were directly used in this study. For stable transfection, PERK and NC shRNAs were cloned into the pENTR/U6-GFP vector containing GFP, followed by recombination between the pENTR/U6-shRNA-GFP and the pLenti6/Block-it-DEST vector. The resultant vector and package plasmid were co-transfected into HEK 293T cells, and viral particles were collected after 48 h. LN229 cells were then infected with lentiPERK shRNA or NC vector, and cells expressing GFP were chosen for further culture.

2.14 Western Blotting

Antibodies used for Western blotting were as follows: anti-PERK (Santa Cruz Biotechnology, Inc., cat. no. sc-13073, 1:100, Dallas, TX, USA), anti-p-PERK (Thr981) (Santa Cruz Biotechnology, Inc., cat. no. sc-32577, 1:100, Dallas, TX, USA), anti-β-ACTIN (Santa Cruz Biotechnology, Inc., cat. no. sc-8432, 1:100, Dallas, TX, USA), anti-E-cadherin (Abcam, cat. no. ab231303, 1:1000, Shanghai, China), anti-N-cadherin (Santa Cruz Biotechnology, Inc., cat. no. SC-53488, 1:200, Dallas, TX, USA), and anti-Vimentin (Abcam, cat. no. ab92547, 1:1000, Shanghai, China). The tissue homogenate or the harvested cells were lysed in protein lysis buffer containing PMSF on an ice bath, and centrifuged. The supernatant was used for protein quantification by the BCA method. A 10–100 µg of protein in each sample was separated by sodium dodecyl sulfate-polyacrylamide gel electrophoresis at 300 mA and transferred to the PVDF membrane. The membrane was placed in the blocking solution for 1 h at 37 ℃ and incubated overnight with the primary antibody at 4 ℃ in a refrigerator. The membrane was blocked for 1 h at 37 °C and then incubated overnight with the primary antibody at 4 °C. After washing with TBST, the membrane was subsequently incubated with a goat anti-mouse IgG horseradish peroxidase-conjugated secondary antibody (Beyotime Institute of Biotechnology, cat. no. A0216, 1:1000, Shanghai, China) for 1 h at room temperature. The membrane was rinsed with TBST solution, and an enhanced chemiluminescence reagent was added to detect signals using a versatile iBright CL1500 Imaging System (Thermo Fisher Scientific, Waltham, MA, USA), and semi-quantitative statistical analysis was performed using ImageLab 6.1 (Bio-Rad Laboratories, Hercules, CA, USA).

2.15 Transwell Invasion Assay

The cells were cultured in serum-free medium for 24 h, trypsinized, centrifuged at 1500 rpm for 3 min, and the supernatant was aspirated. The cells were resuspended in phosphate-buffered saline (PBS), the supernatant was discarded following centrifugation, resuspended again in serum-free medium containing 0.1% BSA to a density of 1×10^5 cells/mL. To a 24-well plate, 500 µL of complete medium and 200 µL of cell suspension was added to the prefabricated Matrigel transwell chamber placed in the 24-well plate containing complete medium. The cells were cultured in a 24-well plate incubator for 24 h, and the cells in the upper chamber were removed. The membrane was then fixed in 10% methanol for 30 s and stained with crystal violet for 20 min. The cells were analysed by a microscope (Leica, DMi1, Shanghai, China) and counted after subtracting the background.

2.16 Wound Healing Assay

The cells were seeded on 6-well plates in triplicate. After overnight culture, the cells were transversely scratched in the middle of the well with a pre-sterilized pipette tip. The floating cells were washed with PBS and fresh medium was added. The cells were visualized under a microscope (Leica, DMi1, Shanghai, China) and images were taken every 24 h. Image-Pro Plus 6.0 (Media Cybernetics, Rockville, MD, USA) was used to calculate the scratch area before and after healing was calculated using the IPP software, and the wound closure rate between the different groups was compared. Wound closure rate using the wound contraction ratioformula, defined as (initial area – current area) / initial area $\times$ 100%.

2.17 Subcutaneous Tumor in Nude Mice

Animal experiments were reviewed and approved by the Institutional Animal Care and Use Committee (IACUC) of Shanghai General Hospital (ID:2021SQ054). All experimental procedures involving animals were conducted adhering strictly with with the Guide for the Care and Use of Laboratory Animals (NIH Publication No. 86-23, revised 1985, U.S. National Academy of Sciences), with predefined humane endpoints (tumor volume $\leq$1500 mm^3, ulceration, or body weight loss $\geq$20%). Twelve female BALB/c nude

mice (6-week-old, weighing 18–22 g) were obtained from Beijing Weitong Lihua Laboratory Animal Technology Co., Ltd., China, and were used for the tumor formation assay. These mice were housed under specific pathogen-free conditions in individually ventilated cages with controlled temperature (22 ± 1 ℃), humidity (50 ± 10%), a 12 h light/dark cycle, and ad libitum access to autoclaved food and water. After 1 week of acclimatization, 12 mice were randomly assigned into two groups (n = 6) and were injected subcutaneously with 2×10^6 lenti-NC or lenti-PERK shRNA LN229 stably transfected glioma cells. Implantation in the hip region was preferred due to low vascularity and ease of monitoring. Tumour dimensions were measured using callipers every 3 days, and their volumes were calculated as $0.5 \times \text{length} \times \text{width}^2$. Mice reaching endpoints were euthanized by cervical dislocation under isoflurane anesthesia; the remaining mice were sacrificed on day 30. The specific parameters were as follows: induction at 1.5–2% isoflurane in 100% oxygen at a flow rate of 2 L/min, followed by maintenance at 1–1.5% isoflurane. The tumours were weighed, photographed on a blue background, and then divided into two groups. One group was fixed using 4% paraformaldehyde, embedded in paraffin, and paraffin sections were prepared for immunohistochemistry. The second group of samples was frozen at –80 ℃ and used subsequently to extract total protein for western blot analysis.

2.18 Immunohistochemical Analyses

Tissue samples were fixed with 4% paraformaldehyde, dehydrated in an alcohol gradient, embedded in xylene-treated paraffin, sliced, and heated at 60 ℃ in an oven for 2 h. The slices were dewaxed and hydrated. The antigens were retrieved by placing the slices in the antigen retrieval solution for 10 min under high pressure. After soaking in PBS, the endogenous peroxidase was blocked with 3% H_2O_2 for 15 min at room temperature. The samples were rinsed with PBS at room temperature and incubated with goat serum for 15 min at room temperature, followed by primary antibodies overnight at 4 °C. The specific antibodies and dilutions were as follows: anti-Vimentin (Abcam, cat. no. ab92547, 1:200, Shanghai, China), anti-E-cadherin (Abcam, cat. no. ab231303, 1:200, Shanghai, China), and anti-N-cadherin (Santa Cruz Biotechnology, Inc., cat. no. SC-53488, 1:50, Dallas, TX, USA). The prepared wash buffer was added and stored in the refrigerator at 4 ℃ overnight. The samples were then soaked in PBS, and the prepared horseradish-labelled sheep anti-mouse/rabbit IgG polymer was added and incubated at 37 ℃ for 30 min. Then, the DAB reagent and haematoxylin stain were applied for 3 min, and the slides were rinsed with 1% hydrochloric acid ethanol. The samples were separated, regressed to blue, dehydrated using gradient alcohol, and cleared with xylene. The stained sections were observed under a neutral resin seal microscope and analysed statistically.

2.19 Statistical Analysis

Data are expressed as the mean ± standard error of the mean (SEM) from three different experiments. The significance was evaluated by Student's *t*-test for comparisons between two groups, or one-way analysis of variance (ANOVA) followed by Tukey's post-hoc testfor comparisons among multiple groups using GraphPad Prism 10.5.0 (GraphPad Software, San Diego, CA, USA). A *p*-value of less than 0.05 was considered statistically significant.

3. Results

3.1 Activation of PERK and EMT Pathways in High-Grade Hypoxic Gliomas Correlates With Poor Prognosis

The activation status of hypoxia across different grades of gliomas was initially investigated by GSVA to score glioma samples from the CGGA dataset using hypoxia gene sets from HALLMARKER, and visualizing the results using the scatter plot (Fig. 1A). The hypoxia score in gliomas increases with tumor grade. Next, we divided the glioma samples into high- and low-hypoxia groups. Enrichment analysis of differentially expressed genes showed that the high hypoxia group was enriched in signaling pathways related to ERS and EMT, such as endoplasmic reticulum lumen, extracellular matrix structural constituent, and leukocyte-mediated immunity pathways (Fig. 1B). Further correlation analysis revealed that, compared with low-grade gliomas, the association between hypoxia and the PERK pathway was stronger in high-grade gliomas, suggesting a possible differential activation of the PERK pathway in high-grade gliomas than in low-grade gliomas under hypoxic conditions (Fig. 1C). We further stratified the cohort into high and low PERK groups based on GSVA scores, and observed lower overall survival (OS) in the high PERK group (Fig. 1D).

3.2 High Activation of the PERK Pathway in Gliomas Enhances EMT-Related Pathways

We conducted differential analysis between high and low PERK score groups to explore whether high activation of PERK in gliomas correlates with EMT (**Supplementary Fig. 1A**). Subsequently, we performed PPI network analysis on significantly upregulated genes in the high PERK activation group, revealing elevated expression of MMP family genes associated with EMT (Fig. 1E). Further GSEA indicated significant enrichment of EMT and hypoxia-related pathways in the high PERK group (Fig. 1F,G). ssGSEA analysis further revealed higher levels of macrophage infiltration in the high PERK group, indicating that PERK activation alters the immune microenvironment of gliomas (**Supplementary Fig. 1B**). Thus, these findings revealed that high-grade gliomas exhibit significantly higher activation in hypoxia, PERK, and EMT pathways than low-grade gliomas (Fig. 1H).

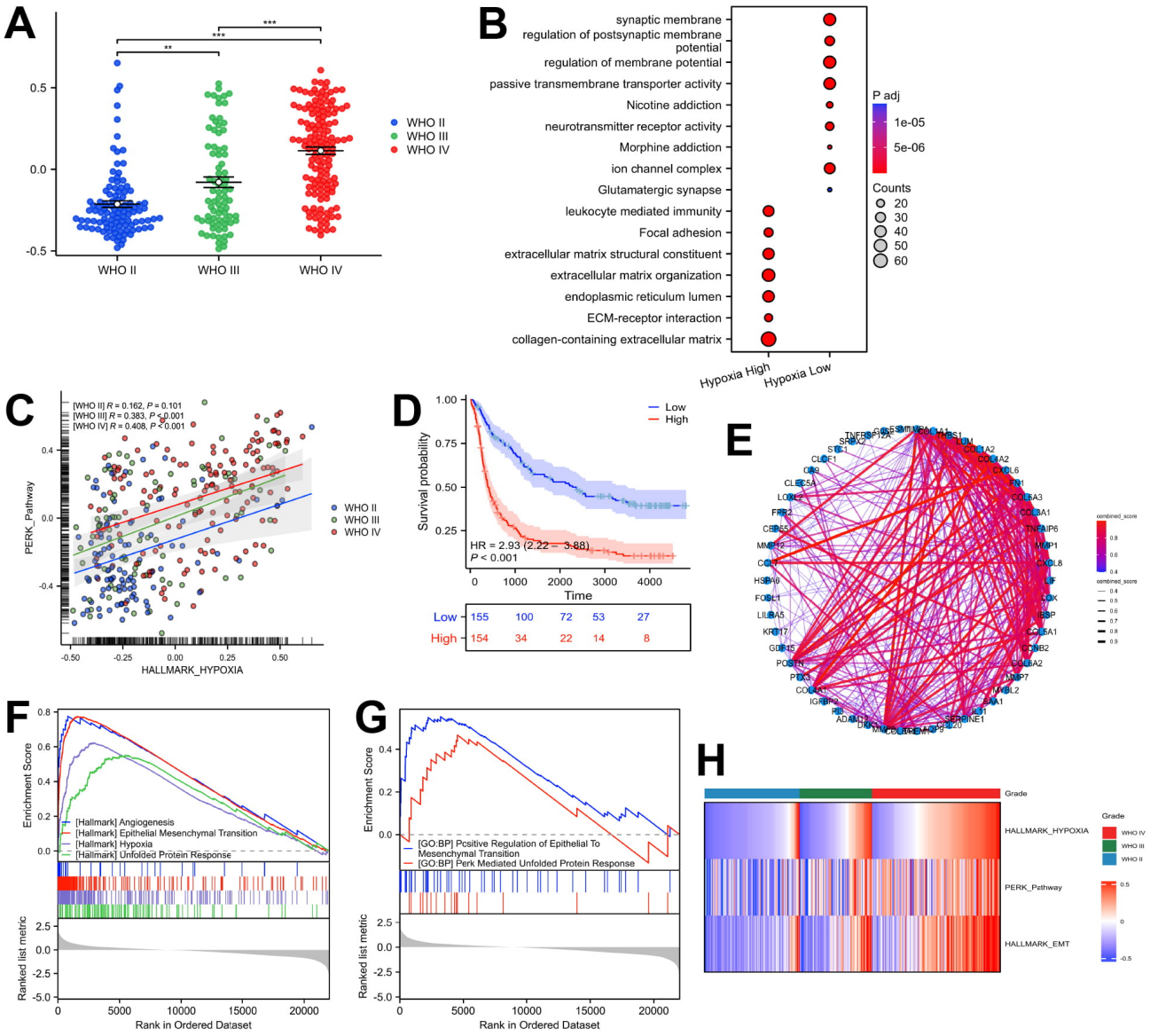

Fig. 1. Bulk transcriptomic analysis showed a correlation between PKR-like endoplasmic reticulum kinase (PERK) pathway activation and epithelial-mesenchymal transition (EMT) in hypoxic gliomas. (A) Scatter plots of hypoxia Gene Set Variation Analysis (GSVA) scores for gliomas of different grades. (B) Enrichment analysis of differentially expressed genes in high- and low-hypoxia groups in glioma. (C) Scatter plot presenting the correlation between hypoxia and PERK score in gliomas of different grades. (D) Survival curve of high- and low-PERK groups in glioma. (E) Protein-Protein Interaction network analysis of the top 100 upregulated genes in the high-PERK activation group. (F,G) Gene Set Enrichment Analysis of differentially expressed genes between high- and low-PERK activation groups. (H) GSVA analysis on gliomas from the Chinese Glioma Genome Atlas (CGGA) dataset and a heatmap to represent the findings. ** $p < 0.01$, *** $p < 0.001$.

3.3 Single-Cell Analysis Reveals Significant Activation of PERK Pathway in Tumor Cells of Glioma

The cellular characteristics and interactions within glioma cells and their tumor microenvironment following PERK activation were examined employing publicly available single-cell sequencing data. We selected two cases each of low-grade and high-grade gliomas for subsequent dimensional reduction clustering to distinguish 11 cell subtypes (Fig. 2A,B, **Supplementary Fig. 1C**). GSVA revealed that compared with low-grade gliomas, high-grade gliomas exhibited significant activation of EMT, hypoxia, and UPR pathways (Fig. 2C). Additionally, Addmodle-Score confirmed significantly higher activation of these pathways in high-grade gliomas than in low-grade gliomas, with a cluster of tumor cell subpopulations only in high-grade gliomas exhibiting a state of hypoxia, PERK, and EMT activation (Fig. 2D–G, **Supplementary Fig. 1D**). This finding is consistent with our previous observations.

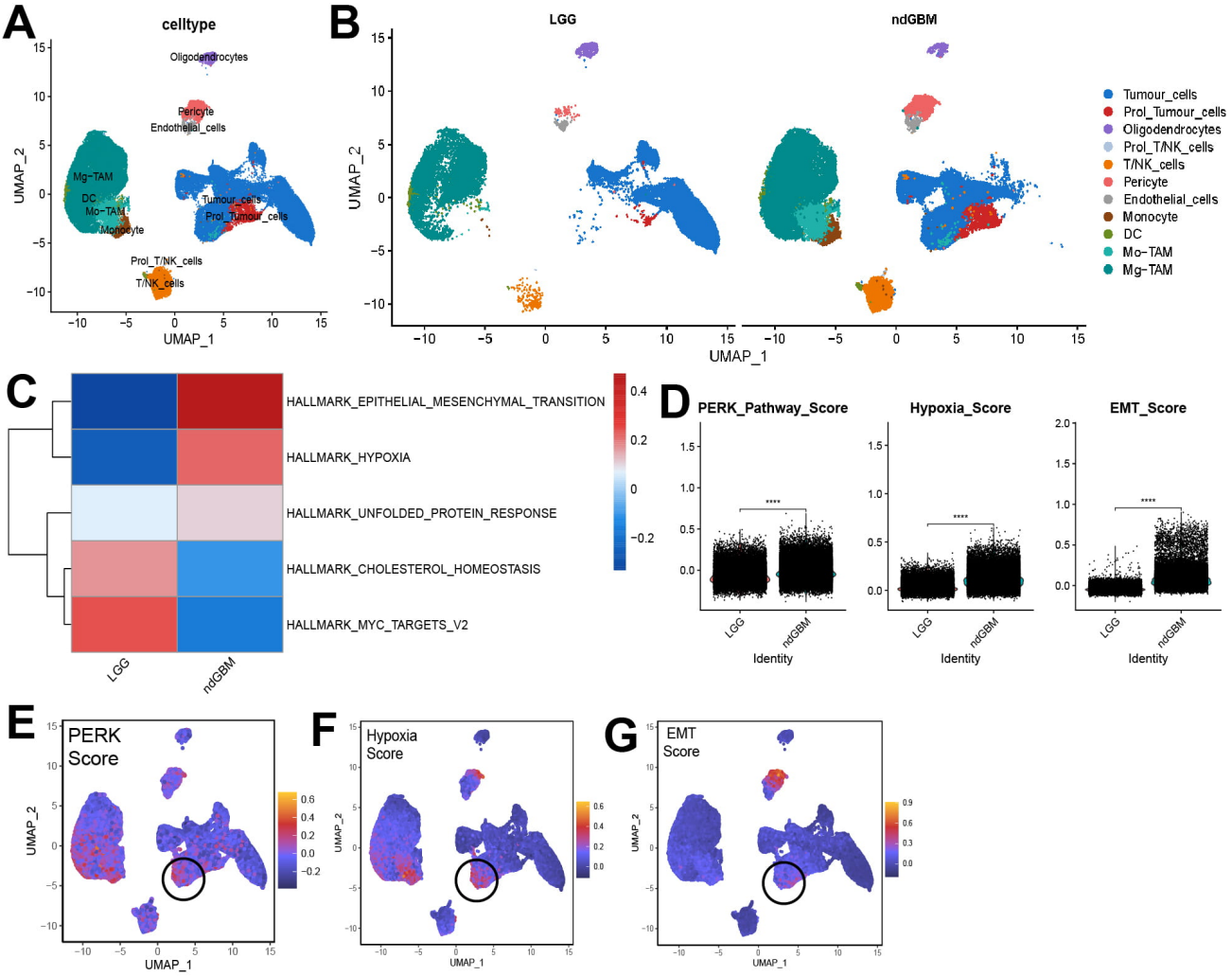

Fig. 2. PKR-like endoplasmic reticulum kinase (PERK), hypoxia and epithelial-mesenchymal transition (EMT) activation in different grades of glioma and cell subpopulations. (A,B) Uniform Manifold Approximation and Projection (UMAP) plots showing annotation of high- and low-grade glioma cells. (C) Gene Set Variation Analysis scoring of high- and low-grade gliomas based on the Hallmark database. (D) Violin plots of AddModuleScore for PERK, hypoxia, and EMT pathways in different grades of gliomas. (E–G) UMAP featureplot of PERK, hypoxia, and EMT pathways scores in gliomas. Black circles highlight tumor cell populations exhibiting high expression of the three specified pathways. **** $p < 0.0001$.

3.4 Pseudo-Temporal Analysis Suggests Increased Expression of EMT-Related Molecules Such as SPP1 in Glioma Cells Upon PERK Activation

Specific tumor subclusters were explored after isolating tumor cells and further subdividing them into AC_like, MES_like, NPC_like, OPC_like, and Prolifeing_Tumor subtypes by their markers. Then we computed the GSVA scores for each tumor subset based on gene sets derived from published literature. The subgroups exhibited the highest enrichment scores corresponding to their respective gene signatures. This consistency supports the validity and reliability of our cell type annotations (**Supplementary Fig. 1E,F** and **Supplementary Table 1**), mesenchymal-like (MES-like) subtype were predominantly present in high-grade gliomas (Fig. 3A,B). The MES-like subtype of tumor cells revealed the highest PERK scoring (Fig. 3C), based on which, we categorized glioma cells into high and low PERK activation groups. The proportion of high PERK activation tumor cells was significantly higher in high-grade gliomas (Fig. 3D). Subsequent GSEA analyses exhibited enhanced activation of EMT, hypoxia, and UPR pathways in the high activation group, further establishing the close association among hypoxia, PERK, and EMT (Fig. 3E,F). Next, a pseudo-temporal analysis was conducted to further investigate the relationship among PERK activation and EMT and hypoxia in glioma cells. The quasi-temporal heatmap simulates the developmental trajectory of the cell (Fig. 3G). At the cellular subtype level, the MES subtype predominantly appeared in the later stages of the pseudo-temporal trajectory, corresponding closely

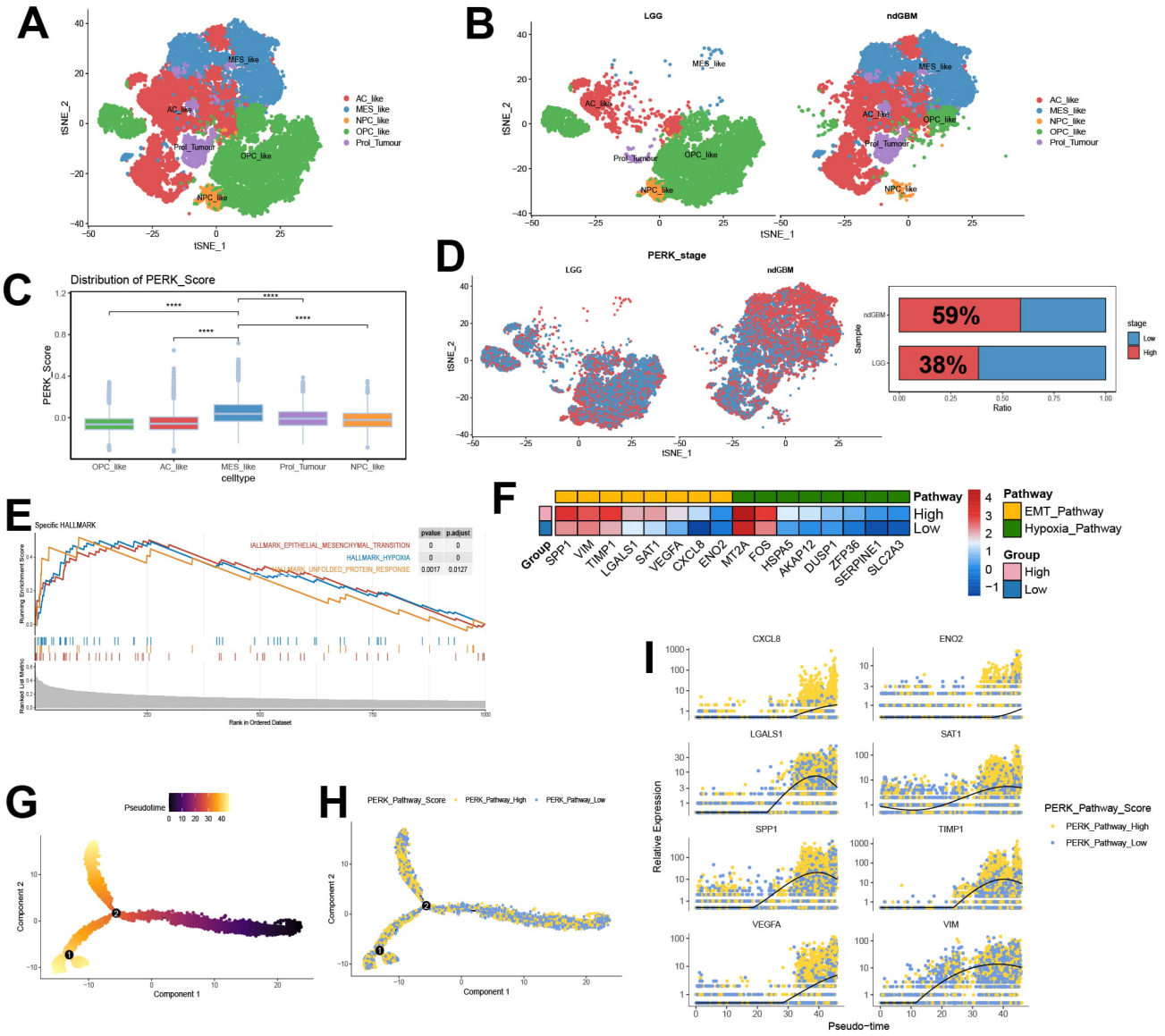

Fig. 3. Single-cell analysis of tumor cell subpopulations shows a strong association between high-PKR-like endoplasmic reticulum kinase (PERK) activation and epithelial-mesenchymal transition (EMT). (A,B) Uniform Manifold Approximation and Projection plots of glioma cell subpopulations in high- and low-grade gliomas. (C) Box plots of AddModuleScore for the PERK pathway in different cell subpopulations. (D) t-Distributed Stochastic Neighbor Embedding (t-SNE) map of glioma cell distribution in high and low PERK pathways. (E) Gene Set Enrichment Analysis of differentially expressed genes between high- and low-PERK pathway glioma tumor cells. (F) A heatmap presenting key gene expression for selected EMT and hypoxia pathways in high- and low-PERK pathway groups. (G,H) A pseudotime heatmap of tumor cells in gliomas. (I) Changes in expression of selected EMT-related genes along the pseudotime developmental axis in gliomas. **** $p < 0.0001$.

to the developmental branch associated with high PERK activation group (Fig. 3H, **Supplementary Fig. 2A,B**). We further examined the distribution of key EMT-related genes across high- and low-PERK activation groups and observed that the transcriptional expression levels of most hypoxia- and EMT-related genes increased with the transition to the high-PERK activation subgroup (Fig. 3I). These results suggest that the activation of the PERK pathway is accompanied by upregulation of EMT-related genes.

3.5 PERK Silencing Lowers the Invasion and Migration Ability of Glioma Cells Under Hypoxia

The role of PERK was further investigated to assess the invasion and migration ability of glioma cells under hypoxic conditions. We first evaluated the effect of PERK knockdown on LN229 cells under hypoxia. Western blot analysis indicated that the knockdown of PERK significantly inhibited the expression of phosphorylated PERK in glioma cells relative to control groups, whereas hypoxic

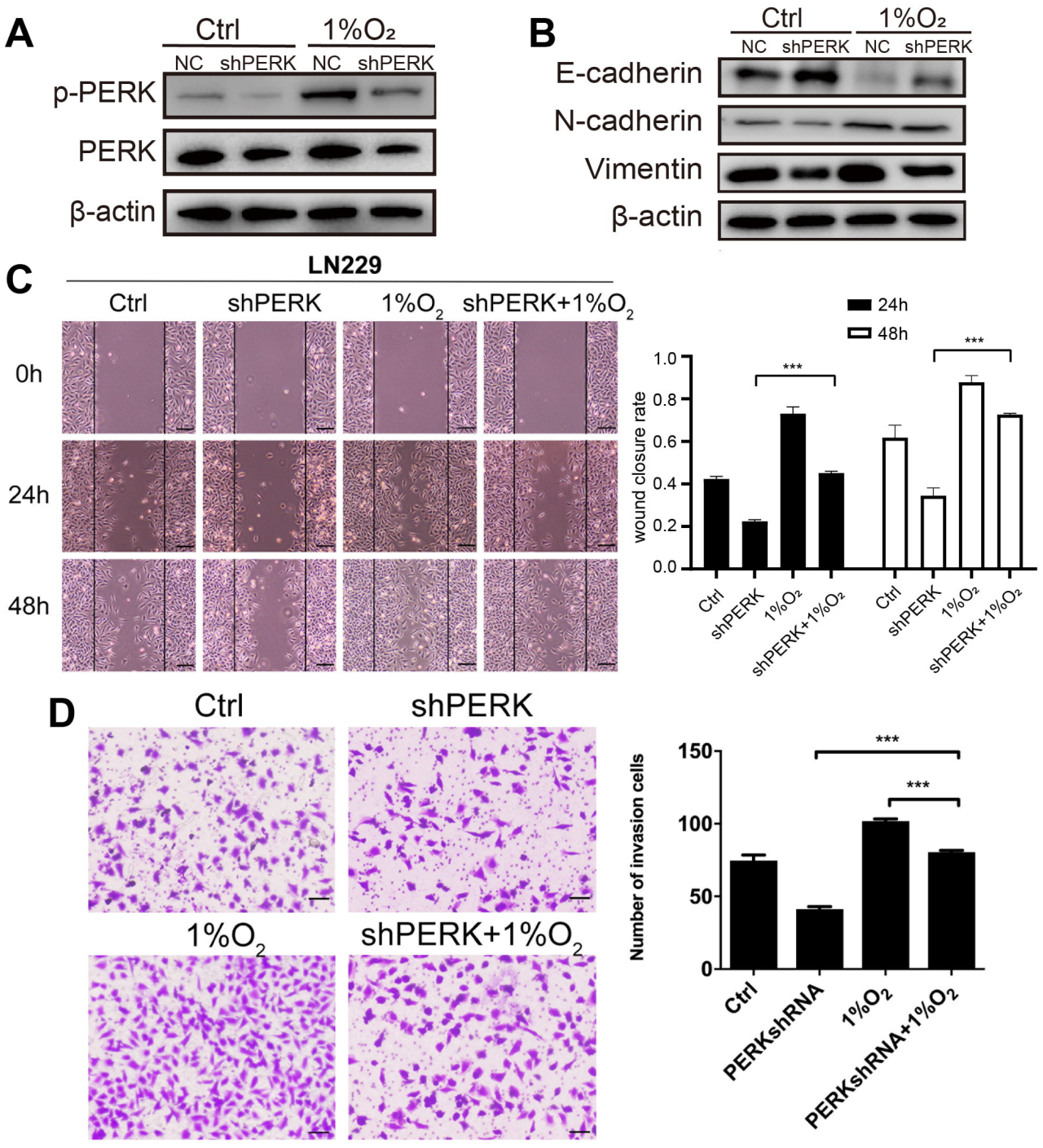

Fig. 4. PKR-like endoplasmic reticulum kinase (PERK) silencing lowers the invasive and migratory ability of glioma cells under hypoxia. LN229 cells were transfected with negative control (NC) or PERK shRNA, and 48 h later, (A) the levels of PERK and phosphorylated (p)-PERK in glioma cells under hypoxia were evaluated by western blotting, (B) the protein levels of epithelial-mesenchymal transition (EMT) in glioma cells under hypoxia were evaluated by western blotting, (C) the migration of glioma cells under hypoxia was quantified using a wound closure rate. Scale bar: 200 μm, and (D) the number of invasive cells was examined by a transwell matrix penetration assay. Scale bar: 80 μm. *** $p < 0.001$. All data are representative of three independent experiments.

conditions partially restored p-PERK levels (Fig. 4A). Our results further demonstrated a reduction in E-cadherin expression, but enhanced vimentin and N-cadherin expression in glioma cells exposed to hypoxic conditions (Fig. 4B). PERK knockdown also inhibited the invasion and migration ability of glioma cells under hypoxia (Fig. 4C,D). Thus, PERK silencing lowered the invasion and migration ability of *in vitro* glioma cells under hypoxia.

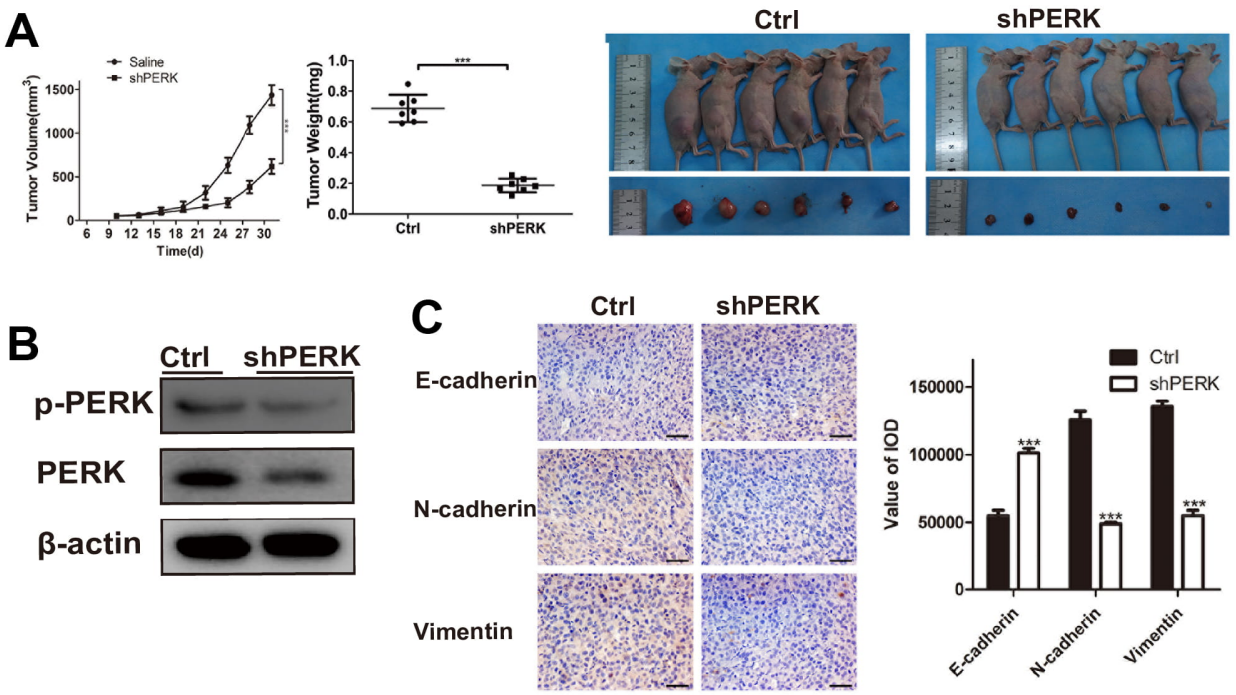

Fig. 5. PKR-like endoplasmic reticulum kinase (PERK) silencing suppresses glioma growth and the epithelial-mesenchymal transition (EMT) process *in vivo* xenografts. (A) Lenti-PERK shRNA and lenti-NC LN229 cells were subcutaneously injected into BALB/c nude female mice. Tumour volume and tumour weights were measured using the *in vivo* proliferation assay. (B) Western blotting was performed for phosphorylated (p)-PERK and PERK *in vivo*. (C) Representative photomicrographs of immunohistochemical analyses for E-cadherin, N-cadherin, and vimentin *in vivo*. Scale bar: 50 µm. *** $p < 0.001$. All data are representative of three independent experiments.

3.6 PERK Silencing Suppresses Glioma Growth In Vivo

The above findings indicate that PERK silencing reduced the invasion and migration ability of glioma cells, likely through modulation of EMT and ER stress-related pathways. However, our *in vitro* data need to be further validated *in vivo*. As glioma cells grow in a hypoxic microenvironment, we hypothesized that PERK silencing may also inhibit glioma invasion and migration *in vivo*, further influencing glioma growth. Consistently, the weights and volumes of the lenti-PERK shRNA tumours were significantly lower than those of control animals (Fig. 5A). Analysis of the expression of related tumor proteins revealed reduced p-PERK protein levels in the PERK-silenced gliomas than those in the control glioma cells (Fig. 5B). Furthermore, immunohistochemical analysis demonstrated decreased levels of vimentin and N-cadherin proteins, along with elevated levels of E-cadherin protein in PERK-silenced gliomas (Fig. 5C). These results suggest that PERK plays an important role in glioma invasion and migration and is associated with EMT and ER stress processes.

3.7 The Hypoxic Regions Enriched PERK-Activated Glioma Cells With the Co-Localization of the EMT Pathway and SPP1-CD44 Signaling

The potential role of PERK-high glioma cells in the tumor immune microenvironment was then explored through a CellChat analysis. Compared with the low PERK group, the high PERK group exhibited significantly enhanced signal outputs (Fig. 6A, **Supplementary Fig. 2C,E**), primarily concentrated in Macrophage migration inhibitory factor (MIF), SPP1, midkine (MK), and VEGF signaling pathways (**Supplementary Fig. 2D**). SPP1 signaling analysis revealed more active interactions between tumor cells with high PERK activity and macrophages than in the low PERK group (Fig. 6B, **Supplementary Fig. 2F**). Using publicly available spatial transcriptomics datasets, we analyzed two cases of low-grade and two of high-grade glioma samples. Hypoxic regions in the glioma were identified using the AddModuleScore, followed by differential gene expression and enrichment analyses (**Supplementary Fig. 2G**). These hypoxic regions were enriched for focal adhesion, endoplasmic reticulum lumen, and undold protein binding pathways, consistent with our bulk RNA-seq findings (Fig. 6C). Using SPOTlight, we deconvoluted single-cell data into spatial transcriptomics data and found that tumor cells with high PERK activation were more abundant in high-grade gliomas, whereas low PERK macrophages were more abundant in low-grade gliomas, even in the same GBM tissue, the tumor cells with high PERK expression were closer to the tumor core area, while the tumor cells with low PERK expression were located at the tumor border (Fig. 6D, **Supplementary Fig. 2H**). Spatial feature

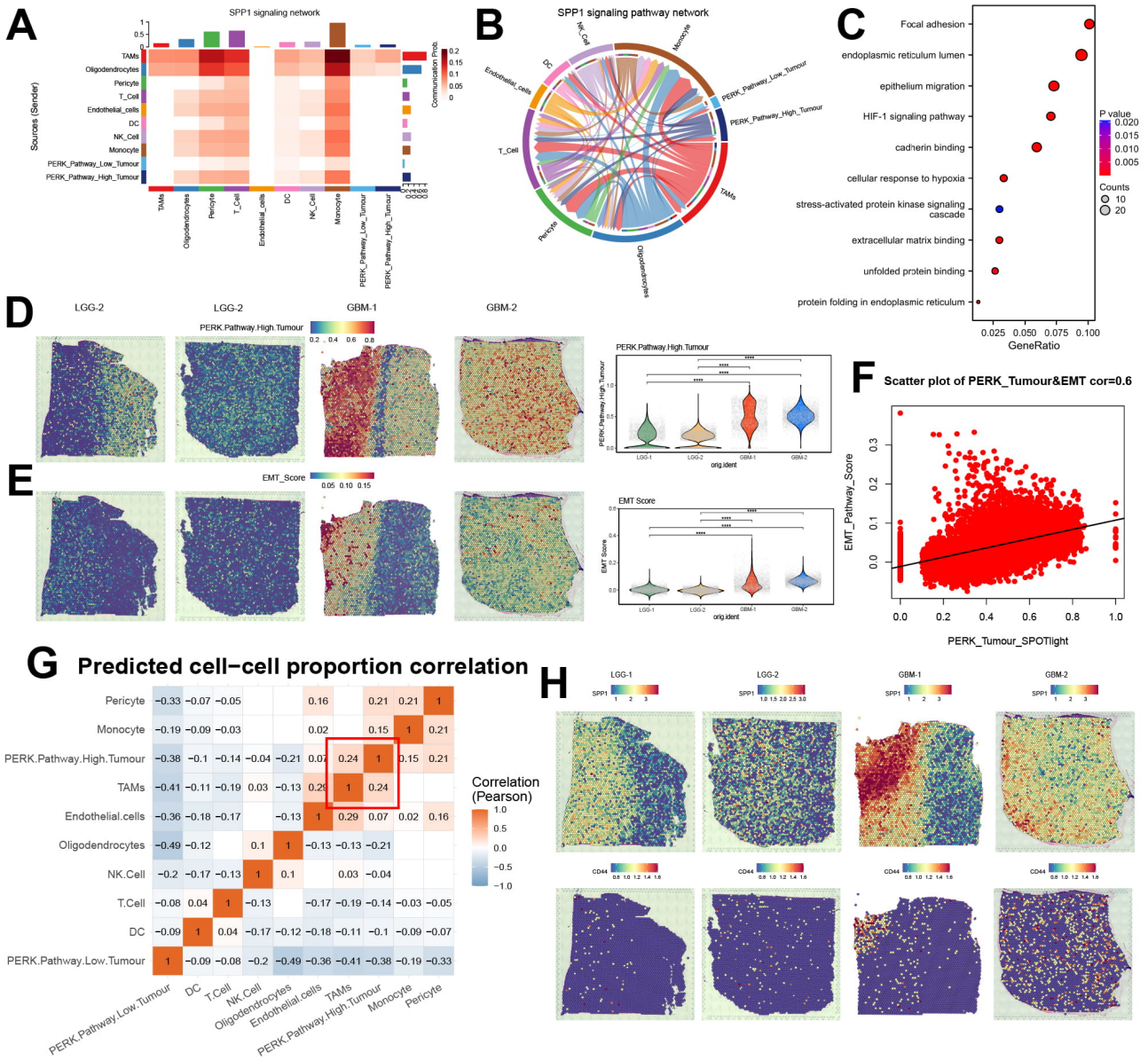

Fig. 6. Spatial transcriptomics and cell communication analyses suggest that tumor cells with high PKR-like endoplasmic reticulum kinase (PERK) activation may induce epithelial-mesenchymal transition (EMT) by enhancing secreted phosphoprotein 1 (SPP1)-CD44 signaling. (A) Heatmap of cell communication signaling via SPP1 in gliomas. (B) A Chordal diagram of SPP1 signal communication between glioma cells. (C) Enrichment analysis of hypoxic niche and other regional differential genes in the spatial transcriptome. (D) A feature map of high PERK activation glioma cells after SPOTLight deconvolution analysis. (E) Spatial feature map of EMT in glioma tissues. (F) Scatter plot showing the spatial correlation between high PERK activation glioma cells and the EMT pathway. (G) A heatmap of spatial cell communication correlations in glioma tissues. (H) Spatial distribution feature map of SPP1 and CD44 in glioma tissues. **** $p < 0.0001$.

mapping of the EMT pathway using AddModuleScore and subsequent correlation analysis revealed that regions with denser distribution of high PERK activation glioma cells exhibited elevated EMT (Fig. 6E,F, cor = 0.6). Finally, we examined the spatial correlation between PERK-HIGH gliomas and TAMs and found a strong correlation between them (Fig. 6G, **Supplementary Fig. 2I**). Furthermore, regions enriched in PERK-high glioma cells also exhibited high expression of SPP1 and CD44, suggesting spatial consistency of this signaling axis (Fig. 6H).

4. Discussion

Glioma, the most common cancer of the central nervous system, characterizes high metabolic activity, resulting in a prevalent hypoxic stress environment within tumor tissues [3]. This hypoxic condition overwhelms or dis-

rupts protein folding functions in the endoplasmic reticulum, leading to ERS [36]. EMT, regulating cell adhesion, migration, and invasion, is frequently observed in cancer, and is often associated with the hypoxic tumor microenvironment [4,37]. In our study, analysis of the CGGA database revealed significant activation of hypoxia, PERK, and EMT pathways in high-grade gliomas. Single-cell sequencing revealed pronounced PERK pathway activation in MES-like glioma cells, concurrent with EMT pathway activation during the transition to the MES subtype. PERK silencing inhibited EMT, leading to a significant reduction in glioma cell invasion and migration. *In vivo* models further confirmed that PERK silencing had an inhibitory effect on glioma growth, an effect partially mediated by decreased EMT activity. In addition, glioma cells with high PERK activation showed stronger cellular crosstalk with TAMs. Spatial transcriptomics confirmed the spatial colocalization of aforementioned molecules, signaling pathways, and cell subtypes. These findings collectively suggest that ERS can affect glioma cell invasion and migration by regulating the EMT process, thus affecting the malignancy of glioma cells.

As the grade of glioma increases, the tumor core becomes highly hypoxic and necrotic, reshaping the immune cell microenvironment, including macrophages [38]. Hypoxia places glioma cells under stress, reducing the capacity of the ER, leading to the accumulation of unfolded or misfolded proteins [11]. Consistent with previous research, we initially analyzed bulk glioma data from the CGGA database and observed a significantly higher activation of hypoxia pathways in high-grade gliomas than in low-grade ones. Additionally, the PERK pathway was significantly activated at the transcriptional level in high-grade gliomas, suggesting that the hypoxic environment within glioma tissues can activate the PERK pathway, which may enhance glioma cell survival under low-oxygen conditions.

Glioblastomas are challenging to cure and often recur within 8 months post-surgery, and EMT, a hallmark of invasiveness, is significantly activated at both the transcriptional and protein levels in glioblastomas [1,2]. Using the REACTOME database and applying GSVA scoring, we categorized glioma cells into high- and low-PERK activation groups, and conducted differential gene expression and enrichment analyses. Glioma tissues in the high PERK-activation group exhibited significant enrichment of hypoxia and EMT pathways, underscoring their interrelation.

Single-cell sequencing, a powerful tool for exploring tumor heterogeneity, revealed that the MES subtype exhibits the highest PERK activation levels. The MES subtype is characterized by high metabolic activity, hypoxia, and aggressive invasiveness [39,40]. A study has suggested that this subtype predominates in the core regions of gliomas, where it promotes macrophage polarization and enhances glioma invasiveness [38]. Our study is the first to identify the highest PERK activation levels in the MES subtype of glioma cells, suggesting that PERK silencing may be a potential target to reduce glioma invasion and treat gliomas. Employing the AddModuleScore method, we subdivided glioma cell subtypes into those with high- and low-PERK activation. The subset with high PERK activation exhibited pronounced hypoxia, elevated EMT, and increased angiogenesis, consistent with our bulk RNA-seq findings. Next, pseudo-time analysis indicated that both the MES subtype and the high PERK activation subset of cells occur predominantly at the end stage of pseudo-time glioma development, aligning with prior research. Genes such as SPP1 and VEGFA, associated with EMT and hypoxia, were also upregulated towards the end of pseudo-time points, suggesting concurrent activation with PERK. The literature also demonstrates that PERK activation in gliomas can regulate angiogenesis through multiple signaling pathways, including VEGFA [41,42]; this pathway has been shown to upregulate SPP1 in smooth muscle cells [43]. Our analysis highlights the role of PERK activation in shaping glioma subtypes and highlights potential therapeutic targets for mitigating glioma invasiveness.

PERK knockdown using lentiviral shRNA revealed a decrease in the expression of p-PERK, accompanied by a reduction in EMT-related protein levels. These molecular changes were functionally validated through *in vitro* invasion and migration assays, which showed impaired cell motility and invasiveness in PERK-silenced glioma cells. *In vivo*, subcutaneous tumor implantation experiments in nude mice further substantiated these findings. PERK knockdown resulted in significantly diminished tumor size and weight compared to control groups, highlighting the role of PERK in sustaining tumor growth and progression. Western blot analysis of tumor tissues confirmed sustained suppression of p-PERK. Additionally, immunohistochemical analysis revealed decreased vimentin and N-cadherin staining alongside increased E-cadherin in PERK-silenced tumors, suggesting that PERK inhibition not only attenuates tumor growth but also promotes less aggressive state.

Given the influence of PERK on the tumor microenvironment, further analysis of the glioma immune microenvironment using CellChatindicated markedly upregulated signals for MIF, SPP1, and VEGF in the high PERK activation group. MIF is currently recognized as an upstream regulator of PERK in the UPR signaling pathway [44], PERK itself can modulate angiogenesis in various malignant tumors through the VEGF signaling [41,45]. SPP1-positive macrophages are now acknowledged to promote cancer progression and suppress immune responses in hepatocellular carcinoma, head and neck squamous cell carcinoma, and other cancers [23,46,47]. A high expression of SPP1 in gliomas has also been shown to be a poor prognostic indicator [48,49]. Therefore, gliomas with high PERK activation may have enhanced invasion through various signaling pathways, promoting macrophage polarization to-

ward an M2-type and contributing to a pro-tumorigenic immune microenvironment.

Finally, spatial transcriptomics analysis further corroborated with these findings. Deconvolution analysis revealed that cells with high PERK activation are predominantly localized in GBM regions. Spatial cell communication analysis further showed a close interconnection between glioma cells with high PERK activation and TAMs, corroborating our earlier hypotheses. Additionally, correlation analysis showed a strong correlation (cor = 0.6) between EMT and glioma cells with high PERK activation, consistent with our previous findings. The spatial distribution of SPP1 and CD44 closely overlapped with the distribution of glioma cells with high PERK activation, underscoring the reliability of our cell communication analyses.

Our research highlights the critical role of PERK in glioma invasion and migration, highlighting its association with EMT and ERS pathways. Additionally, this study also revealed significant variation in PERK activation among different glioma cell subtypes for precision therapy considerations. Our pioneering use of spatial transcriptomics to investigate the relationship between PERK and EMT significantly strengthens the credibility of our previous findings. Nonetheless, this study has limitations. First, we did not examine whether PERK silencing leads to of the suppression of the SPP1 signaling pathway. Second, further research is needed to elucidate the precise molecular mechanisms and clinical applications of PERK silencing. Future studies involving larger spatial transcriptomics cohorts or orthogonal validation using techniques like multiplexed immunofluorescence or flow cytometry will be essential to confirm the robustness and prevalence of the PERK/SPP1/CD44 spatial interaction network across a wider population of gliomas. Third, the 24-hour interval used in our wound healing assays, while optimized for measurable differences under hypoxia and PERK knockdown conditions, may limit the resolution of dynamic changes, future studies could benefit from more frequent time-point imaging. Moving forward, addressing these limitations will be essential for advancing our understanding of the role of PERK in glioma progression and its potential therapeutic implications.

In summary, our study demonstrates that under hypoxic conditions, PERK activation promotes EMT in glioma cells possibly through signaling pathways such as SPP1, facilitating glioma invasion and migration. These data provide evidence supporting PERK silencing as a potential target for glioma treatment, potentially through blocked EMT activation and reducing invasion and migration.

5. Conclusions

Our study demonstrates that hypoxia-induced PERK activation drives EMT in glioma, establishing a critical link between endoplasmic reticulum stress and tumor progression. Integrated multi-omics analyses, functional assays, and spatial transcriptomics consistently show that the PERK-EMT axis promotes invasion. Our findings identify PERK and its associated signaling network as promising therapeutic targets for countering glioma aggressiveness, providing a mechanistic basis for future translational interventions.

Availability of Data and Materials

The data that support the findings of this study are available from the corresponding author upon reasonable request.

Author Contributions

LG and JY designed the experiment, interpreted the data, and wrote the manuscript. JG and YK performed bioinformatic analysis, interpreted the results. XW and HT performed research and contributed reagents. YL and TZ contributed to literature search, draft and revising the manuscript and created figures for the manuscript. JG and YK contributed equally to this manuscript. All authors read and approved the final manuscript. All authors contributed to editorial changes in the manuscript. All authors have participated sufficiently in the work and agreed to be accountable for all aspects of the work.

Ethics Approval and Consent to Participate

Animal experiments were reviewed and approved by the Institutional Animal Care and Use Committee (IACUC) of Shanghai General Hospital (ID:2021SQ054). All experimental procedures involving animals were conducted adhering strictly with the Guide for the Care and Use of Laboratory Animals (NIH Publication No. 86-23, revised 1985, U.S. National Academy of Sciences), with predefined humane endpoints (tumor volume $\leq$1500 mm^3, ulceration, or body weight loss $\geq$20%).

Acknowledgment

Not applicable.

Funding

The present study was supported by the Songjiang District science and technology research project (Grant No.18sjkjgg19, No.18sjkjgg20, and No.18sjkjgg34).

Conflict of Interest

The authors declare no conflict of interest.

Supplementary Material

Supplementary material associated with this article can be found, in the online version, at https://doi.org/10.31083/FBL46692.

References

[1] Wen PY, Packer RJ. The 2021 WHO Classification of Tumors of the Central Nervous System: clinical implications. Neuro-oncology. 2021; 23: 1215–1217. https://doi.org/10.1093/neuonc/noab120.

[2] Weller M, van den Bent M, Preusser M, Le Rhun E, Tonn JC, Minniti G, *et al*. EANO guidelines on the diagnosis and treatment of diffuse gliomas of adulthood. Nature Reviews. Clinical Oncology. 2021; 18: 170–186. https://doi.org/10.1038/s41571-020-00447-z.

[3] Kalluri AL, Shah PP, Lim M. The Tumor Immune Microenvironment in Primary CNS Neoplasms: A Review of Current Knowledge and Therapeutic Approaches. International Journal of Molecular Sciences. 2023; 24: 2020. https://doi.org/10.3390/ijms24032020.

[4] Charles NA, Holland EC, Gilbertson R, Glass R, Kettenmann H. The brain tumor microenvironment. Glia. 2011; 59: 1169–1180. https://doi.org/10.1002/glia.21136.

[5] Hetz C, Zhang K, Kaufman RJ. Mechanisms, regulation and functions of the unfolded protein response. Nature Reviews. Molecular Cell Biology. 2020; 21: 421–438. https://doi.org/10.1038/s41580-020-0250-z.

[6] Lamouille S, Xu J, Derynck R. Molecular mechanisms of epithelial-mesenchymal transition. Nature Reviews. Molecular Cell Biology. 2014; 15: 178–196. https://doi.org/10.1038/nrm3758.

[7] Kalluri R, Weinberg RA. The basics of epithelial-mesenchymal transition. The Journal of Clinical Investigation. 2009; 119: 1420–1428. https://doi.org/10.1172/JCI39104.

[8] Rankin EB, Giaccia AJ. Hypoxic control of metastasis. Science. 2016; 352: 175–180. https://doi.org/10.1126/science.aaf4405.

[9] Kubelt C, Hattermann K, Sebens S, Mehdorn HM, Held-Feindt J. Epithelial-to-mesenchymal transition in paired human primary and recurrent glioblastomas. International Journal of Oncology. 2015; 46: 2515–2525. https://doi.org/10.3892/ijo.2015.2944.

[10] Fan P, Zhang N, Candi E, Agostini M, Piacentini M, TOR Centre, *et al*. Alleviating hypoxia to improve cancer immunotherapy. Oncogene. 2023; 42: 3591–3604. https://doi.org/10.1038/s41388-023-02869-2.

[11] Madden E, Logue SE, Healy SJ, Manie S, Samali A. The role of the unfolded protein response in cancer progression: From oncogenesis to chemoresistance. Biology of the Cell. 2019; 111: 1–17. https://doi.org/10.1111/boc.201800050.

[12] Yang Z, Matteson EL, Goronzy JJ, Weyand CM. T-cell metabolism in autoimmune disease. Arthritis Research & Therapy. 2015; 17: 29. https://doi.org/10.1186/s13075-015-0542-4.

[13] Read A, Schröder M. The Unfolded Protein Response: An Overview. Biology. 2021; 10: 384. https://doi.org/10.3390/biology10050384.

[14] Saini KK, Chaturvedi P, Sinha A, Singh MP, Khan MA, Verma A, *et al*. Loss of PERK function promotes ferroptosis by downregulating SLC7A11 (System Xc^-) in colorectal cancer. Redox Biology. 2023; 65: 102833. https://doi.org/10.1016/j.redox.2023.102833.

[15] Walter P, Ron D. The unfolded protein response: from stress pathway to homeostatic regulation. Science. 2011; 334: 1081–1086. https://doi.org/10.1126/science.1209038.

[16] Talukdar G, Orr HT, Lei Z. The PERK pathway: beneficial or detrimental for neurodegenerative diseases and tumor growth and cancer. Human Molecular Genetics. 2023; 32: 2545–2557. https://doi.org/10.1093/hmg/ddad103.

[17] Ricciardi CA, Gnudi L. The endoplasmic reticulum stress and the unfolded protein response in kidney disease: Implications for vascular growth factors. Journal of Cellular and Molecular Medicine. 2020; 24: 12910–12919. https://doi.org/10.1111/jcmm.15999.

[18] Liu Y, Chen P, Xu L, Wang B, Zhang S, Wang X. GALNT2 sustains glioma stem cells by promoting CD44 expression. Aging. 2023; 15: 2208–2220. https://doi.org/10.18632/aging.204609.

[19] Zhang H, Cao H, Luo H, Zhang N, Wang Z, Dai Z, *et al*. RUNX1/CD44 axis regulates the proliferation, migration, and immunotherapy of gliomas: A single-cell sequencing analysis. Frontiers in Immunology. 2023; 14: 1086280. https://doi.org/10.3389/fimmu.2023.1086280.

[20] Ozato Y, Kojima Y, Kobayashi Y, Hisamatsu Y, Toshima T, Yonemura Y, *et al*. Spatial and single-cell transcriptomics decipher the cellular environment containing HLA-G+ cancer cells and SPP1+ macrophages in colorectal cancer. Cell Reports. 2023; 42: 111929. https://doi.org/10.1016/j.celrep.2022.111929.

[21] Nallasamy P, Nimmakayala RK, Karmakar S, Leon F, Seshacharyulu P, Lakshmanan I, *et al*. Pancreatic Tumor Microenvironment Factor Promotes Cancer Stemness via SPP1-CD44 Axis. Gastroenterology. 2021; 161: 1998–2013.e7. https://doi.org/10.1053/j.gastro.2021.08.023.

[22] Luo H, Xia X, Huang LB, An H, Cao M, Kim GD, *et al*. Pan-cancer single-cell analysis reveals the heterogeneity and plasticity of cancer-associated fibroblasts in the tumor microenvironment. Nature Communications. 2022; 13: 6619. https://doi.org/10.1038/s41467-022-34395-2.

[23] Qi J, Sun H, Zhang Y, Wang Z, Xun Z, Li Z, *et al*. Single-cell and spatial analysis reveal interaction of FAP^+ fibroblasts and $SPP1^+$ macrophages in colorectal cancer. Nature Communications. 2022; 13: 1742. https://doi.org/10.1038/s41467-022-29366-6.

[24] You G, Zheng Z, Huang Y, Liu G, Luo W, Huang J, *et al*. scRNA-seq and proteomics reveal the distinction of M2-like macrophages between primary and recurrent malignant glioma and its critical role in the recurrence. CNS Neuroscience & Therapeutics. 2023; 29: 3391–3405. https://doi.org/10.1111/cns.14269.

[25] Zhao Z, Zhang KN, Wang Q, Li G, Zeng F, Zhang Y, *et al*. Chinese Glioma Genome Atlas (CGGA): A Comprehensive Resource with Functional Genomic Data from Chinese Glioma Patients. Genomics, Proteomics & Bioinformatics. 2021; 19: 1–12. https://doi.org/10.1016/j.gpb.2020.10.005.

[26] Barrett T, Wilhite SE, Ledoux P, Evangelista C, Kim IF, Tomashevsky M, *et al*. NCBI GEO: archive for functional genomics data sets–update. Nucleic Acids Research. 2013; 41: D991–5. https://doi.org/10.1093/nar/gks1193.

[27] Abdelfattah N, Kumar P, Wang C, Leu JS, Flynn WF, Gao R, *et al*. Single-cell analysis of human glioma and immune cells identifies S100A4 as an immunotherapy target. Nature Communications. 2022; 13: 767. https://doi.org/10.1038/s41467-022-28372-y.

[28] Subramanian A, Tamayo P, Mootha VK, Mukherjee S, Ebert BL, Gillette MA, *et al*. Gene set enrichment analysis: a knowledge-based approach for interpreting genome-wide expression profiles. Proceedings of the National Academy of Sciences of the United States of America. 2005; 102: 15545–15550. https://doi.org/10.1073/pnas.0506580102.

[29] Liberzon A, Subramanian A, Pinchback R, Thorvaldsdóttir H, Tamayo P, Mesirov JP. Molecular signatures database (MSigDB) 3.0. Bioinformatics. 2011; 27: 1739–1740. https://doi.org/10.1093/bioinformatics/btr260.

[30] Jassal B, Matthews L, Viteri G, Gong C, Lorente P, Fabregat A, *et al*. The reactome pathway knowledgebase. Nucleic Acids Research. 2020; 48: D498–D503. https://doi.org/10.1093/nar/gkz1031.

[31] Szklarczyk D, Kirsch R, Koutrouli M, Nastou K, Mehryary F, Hachilif R, *et al*. The STRING database in 2023: protein-protein

association networks and functional enrichment analyses for any sequenced genome of interest. Nucleic Acids Research. 2023; 51: D638–D646. https://doi.org/10.1093/nar/gkac1000.

[32] Bindea G, Mlecnik B, Tosolini M, Kirilovsky A, Waldner M, Obenauf AC, *et al*. Spatiotemporal dynamics of intratumoral immune cells reveal the immune landscape in human cancer. Immunity. 2013; 39: 782–795. https://doi.org/10.1016/j.immuni.2013.10.003.

[33] Neftel C, Laffy J, Filbin MG, Hara T, Shore ME, Rahme GJ, *et al*. An Integrative Model of Cellular States, Plasticity, and Genetics for Glioblastoma. Cell. 2019; 178: 835–849.e21. https://doi.org/10.1016/j.cell.2019.06.024.

[34] Qiu X, Hill A, Packer J, Lin D, Ma YA, Trapnell C. Single-cell mRNA quantification and differential analysis with Census. Nature Methods. 2017; 14: 309–315. https://doi.org/10.1038/nmeth.4150.

[35] Jin S, Guerrero-Juarez CF, Zhang L, Chang I, Ramos R, Kuan CH, *et al*. Inference and analysis of cell-cell communication using CellChat. Nature Communications. 2021; 12: 1088. https://doi.org/10.1038/s41467-021-21246-9.

[36] Elhanani O, Ben-Uri R, Keren L. Spatial profiling technologies illuminate the tumor microenvironment. Cancer Cell. 2023; 41: 404–420. https://doi.org/10.1016/j.ccell.2023.01.010.

[37] Pavlova NN, Zhu J, Thompson CB. The hallmarks of cancer metabolism: Still emerging. Cell Metabolism. 2022; 34: 355–377. https://doi.org/10.1016/j.cmet.2022.01.007.

[38] Greenwald AC, Darnell NG, Hoefflin R, Simkin D, Mount CW, Gonzalez Castro LN, *et al*. Integrative spatial analysis reveals a multi-layered organization of glioblastoma. Cell. 2024; 187: 2485–2501.e26. https://doi.org/10.1016/j.cell.2024.03.029.

[39] Verhaak RGW, Hoadley KA, Purdom E, Wang V, Qi Y, Wilkerson MD, *et al*. Integrated genomic analysis identifies clinically relevant subtypes of glioblastoma characterized by abnormalities in PDGFRA, IDH1, EGFR, and NF1. Cancer Cell. 2010; 17: 98–110. https://doi.org/10.1016/j.ccr.2009.12.020.

[40] Hara T, Chanoch-Myers R, Mathewson ND, Myskiw C, Atta L, Bussema L, *et al*. Interactions between cancer cells and immune cells drive transitions to mesenchymal-like states in glioblastoma. Cancer Cell. 2021; 39: 779–792.e11. https://doi.org/10.1016/j.ccell.2021.05.002.

[41] Wang L, Wen J, Sun Y, Yang X, Ma Y, Tian X. Knockdown of NUPR1 inhibits angiogenesis in lung cancer through IRE1/XBP1 and PERK/eIF2α/ATF4 signaling pathways. Open medicine (Warsaw, Poland). 2023; 18, 20230796. https://doi.org/10.1515/med-2023-0796.

[42] Soni H, Bode J, Nguyen CDL, Puccio L, Neßling M, Piro RM, *et al*. PERK-mediated expression of peptidylglycine α-amidating monooxygenase supports angiogenesis in glioblastoma. Oncogenesis. 2020; 9: 18. https://doi.org/10.1038/s41389-020-0201-8.

[43] Kaw K, Chattopadhyay A, Guan P, Chen J, Majumder S, Duan XY, *et al*. Smooth muscle α-actin missense variant promotes atherosclerosis through modulation of intracellular cholesterol in smooth muscle cells. European Heart Journal. 2023; 44: 2713–2726. https://doi.org/10.1093/eurheartj/ehad373.

[44] Poulsen KL, McMullen MR, Huang E, Kibler CD, Sheehan MM, Leng L, *et al*. Novel Role of Macrophage Migration Inhibitory Factor in Upstream Control of the Unfolded Protein Response After Ethanol Feeding in Mice. Alcoholism, Clinical and Experimental Research. 2019; 43: 1439–1451. https://doi.org/10.1111/acer.14065.

[45] Blais JD, Addison CL, Edge R, Falls T, Zhao H, Wary K, Koumeni C, *et al*. Perk-dependent translational regulation promotes tumor cell adaptation and angiogenesis in response to hypoxic stress. Molecular and cellular biology. 2006; 26: 9517–9532. https://doi.org/10.1128/MCB.01145-06.

[46] Bill R, Wirapati P, Messemaker M, Roh W, Zitti B, Duval F, *et al*. *CXCL9:SPP1* macrophage polarity identifies a network of cellular programs that control human cancers. Science. 2023; 381: 515–524. https://doi.org/10.1126/science.ade2292.

[47] Liu Y, Xun Z, Ma K, Liang S, Li X, Zhou S, *et al*. Identification of a tumour immune barrier in the HCC microenvironment that determines the efficacy of immunotherapy. Journal of Hepatology. 2023; 78: 770–782. https://doi.org/10.1016/j.jhep.2023.01.011.

[48] Chen P, Zhao D, Li J, Liang X, Li J, Chang A, *et al*. Symbiotic Macrophage-Glioma Cell Interactions Reveal Synthetic Lethality in PTEN-Null Glioma. Cancer Cell. 2019; 35: 868–884.e6. https://doi.org/10.1016/j.ccell.2019.05.003.

[49] Pietras A, Katz AM, Ekström EJ, Wee B, Halliday JJ, Pitter KL, *et al*. Osteopontin-CD44 signaling in the glioma perivascular niche enhances cancer stem cell phenotypes and promotes aggressive tumor growth. Cell Stem Cell. 2014; 14: 357–369. https://doi.org/10.1016/j.stem.2014.01.005.